

Eigenvalue Method for the Outer-Region Matching Data in Resistive MHD Stability Analysis

TOKUDA Shinji and WATANABE Tomoko*

Department of Fusion Plasma Research,

Naka Fusion Research Establishment, Japan Atomic Energy Research Institute, Ibaraki 311-01, Japan

**Research Organization for Information Science and Technology, Ibaraki 319-11, Japan*

(Received 29 July 1997)

Abstract

A new method is presented to compute the outer-region matching data which play a crucial role in resistive MHD stability analysis in a tokamak plasma. The method also provides an alternative method for the ideal MHD stability analysis which can identify the marginally stable state. In the present method, an eigenvalue problem is posed for the Newcomb equation, one dimensional marginally stable ideal MHD equation. And then, the finite energy part of the solution for the Newcomb equation is divided into two components: the eigenfunction whose eigenvalue is the nearest to zero and the remainder which is orthogonal to the eigenfunction and satisfies a singular equation. An integral relation by Pletzer-Dewar [J. Plasma Phys. **45**, 427 (1991)] is employed to abstract the matching data from the finite energy part of the solution. Numerical experiments are performed to demonstrate effectiveness of the new method for a model equation with analytical solutions and for the Newcomb equation in the $m = 1$ mode theory (m : poloidal mode number).

Keywords:

Newcomb equation, resistive MHD stability, tokamak, matching data, eigenvalue problem, boundary value problem, singular equation, finite element method

1. Introduction

The matching data play a crucial role in the linear and nonlinear stability analyses of resistive MagnetoHydroDynamic modes in a tokamak plasma. In resistive MHD stability analysis, the plasma is divided into two regions [1, 2]. In the outer region far from rational surfaces, the plasma can be described by the ideal MHD equation without inertia. The equation in this region, called the Newcomb equation [3], has regular singular points at the rational surfaces. In the thin inner layer around a rational surface, all dynamics such as inertia, electrical resistivity and viscosity must be retained. However, equations of motion can be substantially reduced in the inner layer. The solutions in both regions are asymptotically matched and then the nonideal MHD motion of the plasma is determined. The quantities to be matched are called matching data.

A reliable numerical method has not been available before the advent of the paper by Pletzer and Dewar [4]. The Newcomb equation is homogeneous and the solution is expressed as the linear combination of the square integrable solution (small solution) and the non square integrable solution (big solution) around a rational surface. In ref. [4] the problem is reformulated as a boundary value problem of an inhomogeneous equation whose solutions are in a set of square integrable functions. The source term in the inhomogeneous equation is constructed from the big solution. This boundary value problem has a quadratic form and the variational principle can be derived. Therefore, a finite element method [5] can be applied for this problem. Their method is applicable to a finite beta plasma in a two dimensional toroidal configuration [6]. However, this method can not be applied when the plasma is

close to the marginal ideal MHD stability because the small solution satisfies the boundary conditions by itself and the Newcomb equation becomes singular for the marginal stability case. An important example is the $m = 1$ mode instability in tokamak plasmas [7, 8].

In the present paper, we propose a new method, termed the eigenvalue method, to compute the outer-region matching data in a one-dimensional problem. We pose an eigenvalue problem for the Newcomb equation instead of the boundary value problem. We divide the finite energy part of the solution into two components: the eigenfunction with the eigenvalue nearest to zero and the remainder orthogonal to the eigenfunction. Then we derive a singular equation for the remainder component. We also derive an integral relation to abstract the matching data.

Except for the case of marginal stability, the eigenvalue method is equivalent to the Pletzer-Dewar method. However, the eigenvalue method has several advantages: it is a new method of ideal MHD stability analysis by which the marginally stable state can be identified, and it guarantees numerical stability in computing matching data when a plasma is close to marginal stability.

In section 2 we give a brief review on the outer-region matching data and the Pletzer-Dewar method. In section 3 we formulate the eigenvalue method to compute the matching data. Here, we discuss the boundary conditions at the rational surface appropriate to the eigenvalue problem and boundary value problem. Such a discussion has not been sufficiently given so far. We also derive the variational principle for the singular equation associated with the eigenvalue equation, which justifies employing the finite element methods. In section 4 we give a proof on the uniqueness of the matching data computed by this method. We verify the present method by applying it to a model equation in section 5, and by using this method we compute the matching data for the $m = 1$ Newcomb equation and compare the results with the $m = 1$ mode theory in section 6. Discussion and conclusions are given in section 7.

2. Outer-Region Matching Data

Let us consider the following boundary value problem:

$$\mathcal{L}\xi \equiv \frac{d}{dx} \left(f(x) \frac{d\xi}{dx} \right) - g(x)\xi = 0, \quad x \in [0, a], \quad (1)$$

$$\xi(x=0) = \xi(x=a) = 0. \quad (2)$$

We assume that Eq.(1) has the regular singular point $x_0 \in (0, a)$ and that the functions $f(x)$ and $g(x)$ can be Taylor expanded around $x = x_0$ as

$$f(x) = f_0(x - x_0)^2 + (x - x_0)^3 + \dots, \\ f_0 > 0, \quad (3)$$

$$g(x) = g_0 + g_1(x - x_0) + \dots, \quad g_0 \neq 0. \quad (4)$$

The Newcomb equation, the one dimensional marginally stable ideal MHD equation [3], has the same form as Eq.(1) and the regular singular point corresponds to the rational surface. In the Newcomb equation the inertia of the plasma is neglected as well as any nonideal effects such as electrical resistivity.

As is well known [4], the regular singular point separates the region $[0, a]$ into the left side region $[0, x_0]$ and the right side region $(x_0, a]$. Equation (1) has two fundamental solutions in each side which can be expressed by the Frobenius series around $x = x_0$ as

$$\xi(x) = |x - x_0|_p^{-1/2 \pm \mu} \sum_{m=0}^{\infty} \xi_m(x - x_0)^m, \\ p = L, R, \quad (5)$$

where $|x - x_0|_R = 0$ ($|x - x_0|_L = 0$) for $x \in [0, x_0]$ ($x \in (x_0, a]$) and $|x - x_0|_R = x - x_0$ ($|x - x_0|_L = x_0 - x$) for $x \in (x_0, a]$ ($x \in [0, x_0]$). In Eq.(5), the index μ , called the Suydam-Mercier index, is given by

$$\mu = \sqrt{\frac{1}{4} + \frac{g_0}{f_0}}. \quad (6)$$

Here we assume that the Suydam stability condition,

$$\frac{1}{4} + \frac{g_0}{f_0} > 0, \quad (7)$$

is satisfied and μ is a positive real number. Therefore, the fundamental solutions, Eq.(5), comprise the "big solution" with the power $-1/2 - \mu$, which is not square integrable, and the "small solution" with the power $-1/2 + \mu$, which is square integrable. The solution $\xi(x)$ of the boundary value problem, Eq.(1), is expressed as

$$\xi(x) = c_L (\xi_L^b(x) + \Delta_L \xi_L^s(x)) + c_R (\xi_R^b(x) + \Delta_R \xi_R^s(x)), \quad (8)$$

where $\xi_p^b(x)$ ($p = L, R$) behaves as the big solution and $\xi_p^s(x)$ behaves as the small solution near the point x_0 . The coefficients Δ_p are the "outer-region matching data" with which we are concerned. They are determined from the boundary condition at $x = 0$ for Δ_L and

at $x = a$ for Δ_R . The coefficients c_p are the undetermined constants.

In the resistive MHD stability analysis, it is more convenient to define $\Delta' = \Delta_R + \Delta_L$ and $\Gamma' = \Delta_R - \Delta_L$ and to express the solution $\xi(x)$ as

$$\xi(x) = c_+ \left[\xi_+^b(x) + \frac{1}{2} (A' \xi_+^s(x) + B' \xi_-^s(x)) \right] + c_- \left[\xi_-^b(x) + \frac{1}{2} (\Gamma' \xi_+^s(x) + \Delta' \xi_-^s(x)) \right], \quad (9)$$

where $\xi_+^\alpha \equiv \xi_R^\alpha + \xi_L^\alpha$ and $\xi_-^\alpha \equiv \xi_R^\alpha - \xi_L^\alpha$ ($\alpha = b$ or s) and $A' = \Delta'$, $B' = \Gamma'$. For example, the dispersion relation for the tearing mode (odd parity mode) is given by

$$\Delta' = \Delta(\omega),$$

where ω is the complex frequency of the mode and the "inner-region matching data" $\Delta(\omega)$ is determined by the solution of the inner layer equations [8].

In the method proposed by Pletzer and Dewar [4], the solution $\xi(x)$ for Eq.(1) is divided into the finite energy part $\zeta_p(x)$ and the infinite energy part $\hat{\xi}_p(x)$ defined by

$$\hat{\xi}_p(x) = H(x) \xi_p^b. \quad (10)$$

Here ξ_p^b is expressed by the Frobenius series, Eq.(5), truncated at finite terms and $H(x)$ is a support function ($H(x_0) = 1$ and $H(x) = 0$ for $|x - x_0| > \epsilon$ and $\epsilon > 0$ is a given constant).

The finite energy part $\zeta_p(x)$ is numerically computed by solving the equation

$$\mathcal{L} \zeta_p(x) = -(\mathcal{L} \hat{\xi}_p(x)), \quad (11)$$

with the same boundary conditions with Eq.(2). The solution $\zeta_p(x)$ behaves as the small solution near the point x_0 and the matching data are abstracted from $\zeta_p(x)$ by using the *bilinear concomitant*. However, this method is not applied when the plasma is close to the marginal ideal MHD stability because the small solution satisfies the boundary conditions by itself to yield $|\Delta_p| = \infty$ and the operator \mathcal{L} becomes singular for this case. As pointed in the paper [9], it is more suitable to express the solution $\xi(x)$ of Eq.(1) as

$$\xi(x) = c_L (\xi_L^s(x) + \Delta_L^{-1} \xi_L^b(x)) + c_R (\xi_R^s(x) + \Delta_R^{-1} \xi_R^b(x)), \quad (12)$$

when the plasma is close to the marginal stability. In the next section we propose a new method to compute the outer-region matching data in the form of Eq.(12). Thus, matching data can be numerically computed for

the plasma close to the marginal stability.

3. Eigenvalue Method

When a plasma is in the marginal stability, Eq.(1) has a nontrivial solution which is square integrable and satisfies the boundary conditions, Eq.(2). To explore such a case from a general point of view, let us consider an eigenvalue problem

$$\mathcal{L} \xi(x) = -\lambda \rho(x) \xi(x), \quad (13)$$

instead of Eq.(1). Here $\xi(x)$ is square integrable and $\rho(x)$ is chosen as

$$\rho(x) = \rho_0 (x - x_0)^2, \quad \rho_0 \in 0. \quad (14)$$

where ρ_0 is a given constant. The Suydam-Mercier index is assumed to be

$$0 < \mu < 1, \quad (15)$$

which will suffice for the almost physical applications.

The quadratic form yielding Eq.(13) by variation is given by

$$W(\xi, \xi) - \lambda \left(\int_0^a \rho(x) |\xi(x)|^2 dx - 1 \right), \quad (16)$$

where the potential energy $W(\xi, \xi)$ is

$$W(\xi, \xi) = \int_0^a \left(f \left| \frac{d\xi}{dx} \right|^2 + g |\xi|^2 \right) dx. \quad (17)$$

In Eq.(16), λ plays the role of the Lagrange multiplier. The bilinear form corresponding to Eq.(17) reads

$$W(\zeta, \xi) = \int_0^a \left(f \frac{d\zeta^*}{dx} \frac{d\xi}{dx} + g \zeta^* \xi \right) dx. \quad (18)$$

where $*$ denotes the complex conjugate, and the bilinear concomitant is given by

$$\zeta^* \mathcal{L} \xi - \xi (\mathcal{L} \zeta)^* = \frac{d}{dx} P[\xi, \zeta; x], \quad (19)$$

$$P[\xi, \zeta; x] \equiv f(x) \left(\zeta^* \frac{d\xi}{dx} - \xi \frac{d\zeta^*}{dx} \right). \quad (20)$$

The proper boundary condition is obtained from Eqs.(19) and (20) for ξ and ζ at the regular singular point x_0 to make the operator \mathcal{L} self-adjoint. Let \mathcal{H} be a set of square integrable functions whose singularity is at most $|x - x_0|^{-1/2+\mu}$ at x_0 . Then we get

$$\lim_{x \rightarrow x_0} f(x) \zeta^* \frac{d\xi}{dx} = 0, \quad \xi, \zeta \in \mathcal{H}, \quad (21)$$

for the function $f(x)$ given by Eq.(3), and the relation

$$(\zeta, \mathcal{L}\xi) = (\mathcal{L}\zeta, \xi)^* , \quad (22)$$

follows for $\xi, \zeta \in \mathcal{H}$, where

$$(f, g) = \int_0^a f^*(x)g(x)dx . \quad (23)$$

Equation (22) means that the operator \mathcal{L} is self-adjoint without boundary conditions for ξ and ζ at the regular singular point as long as they are in \mathcal{H} (natural boundary conditions [10]). Thus the *natural boundary condition* for ξ should be imposed at the regular singular point x_0 when we apply a finite element method for Eq.(16).

We observe several fundamental theorems on the eigenvalue problem, Eq.(13). First, Eq.(13) has two kinds of eigenfunctions $\xi_L(x)$ and $\xi_R(x)$ such that

$$\begin{aligned} \xi_L(x) &\neq 0, \text{ for } 0 < x < x_0, \\ \xi_L(x) &= 0, \text{ for } x_0 < x < a, \\ \text{and} \\ \xi_R(x) &= 0, \text{ for } 0 < x < x_0, \\ \xi_R(x) &\neq 0, \text{ for } x_0 < x < a, \end{aligned}$$

and all eigenfunctions behave as the small solution near the point $x = x_0$ with the same exponent $-1/2 + \mu$. The first two terms in the Frobenius series of all eigenfunctions are the same for the weight function $\rho(x)$ given by Eq.(14). Next, Eq.(13) possesses the classical Sturm-Liouville properties [10]: the spectrum of Eq.(13) comprises real and denumerable eigenvalues that can be ordered in the form of $\lambda_1 \leq \lambda_2 \leq \dots$, any two eigenfunctions ξ_j and ξ_k belonging to different eigenvalues are mutually orthogonal,

$$(\xi_j, \rho\xi_k) = 0 , \quad (24)$$

and arbitrary square integrable function $\zeta(x)$ can be expanded in terms of ξ_j 's,

$$\zeta(x) = \sum_{j=1}^{\infty} c_j \xi_j(x) . \quad (25)$$

Finally, for each eigenfunction ξ_j with the eigenvalue λ_j , the relation

$$W(\xi_j, \xi_j) = \lambda_j , \quad (26)$$

follows provided that $\|\xi_j\|^2 = 1$, where the norm of a function $\xi(x) \in \mathcal{H}$ is defined by

$$\|\xi_j\|^2 \equiv (\xi, \rho\xi) . \quad (27)$$

Therefore, the plasma is marginally stable if the smallest eigenvalue of Eq.(13) is null ($\lambda = 0$), and the plasma is unstable if Eq.(13) has negative eigenvalues

because a square integrable function ξ making the potential energy $W(\xi, \xi)$ negative can be constructed [3]. Consequently, the eigenvalue problem, Eq.(13), with the weight function $\rho(x)$ given by Eq.(14), provides an alternative method of ideal MHD stability analysis, which can identify the marginal stability, whereas the conventional spectral methods cannot [11–13].

In the present eigenvalue problem, it is crucial to choose both the weight function $\rho(x)$ as Eq.(14) and the natural boundary condition at the rational surface. Both of them determine the spectral structure of Eq.(13). If $\rho(x = x_0) > 0$, which is the case in the conventional methods, then the Mercier-Suydam index μ for the eigenfunctions depends on the eigenvalue λ . This allows Eq.(13) to have continuous spectra and the eigenvalue corresponding to the marginally stable state cannot be numerically singled out among them. Moreover, the behavior of eigenfunctions near the regular singular point x_0 differs from that of the small solution of Eq.(1), which will fail the validity of both the above and the following discussions.

Now let us return to Eq.(1). It is convenient to write the solution $\xi(x)$ as

$$\begin{aligned} \xi_p(x) &= \xi_{p,0}(x) + \lambda_0 \zeta_p(x) + \lambda_0 \Omega_p \hat{\xi}_p^b(x) , \\ p &= L, R . \end{aligned} \quad (28)$$

Here $\xi_{p,0}(x)$ is the eigenfunction of Eq.(13) whose eigenvalue λ_0 satisfies $|\lambda_0| = \min |\lambda_j|$ ($j = 1, 2, \dots$) and ζ_p is orthogonal to $\xi_{p,0}(x)$,

$$(\xi_{p,0}, \rho\zeta_p) = 0 . \quad (29)$$

The function ζ_p satisfies the singular equation

$$\mathcal{L}\zeta_p(x) = \rho(x)\xi_{p,0}(x) - \Omega_p \mathcal{L}\hat{\xi}_p^b(x) , \quad (30)$$

with the boundary conditions

$$\zeta_p(x=0) = \zeta_p(x=a) = 0 . \quad (31)$$

The solubility condition for Eq.(30) determines Ω_p to give

$$\Omega_p = \frac{\|\xi_{p,0}\|^2}{(\xi_{p,0}, \mathcal{L}\hat{\xi}_p^b)} , \quad (32)$$

and the solution ζ_p of Eq.(30) satisfies the relation

$$W(\zeta_p, \zeta_p) = \Omega_p (\zeta_p, \mathcal{L}\hat{\xi}_p^b) . \quad (33)$$

The outer-region matching data in Eq.(12) can be computed by using the solution ζ_p as follows. By comparing the finite energy part

$$\xi_f(x) = \xi_{p,0}(x) + \lambda_0 \zeta_p(x), \quad (34)$$

in Eq.(28) with that in Eq.(12), we see $\xi_f(x) = c_f \hat{\xi}_p^s(x)$ and

$$\begin{aligned} \xi_p(x) &= \xi_{p,0}(x) + \lambda_0 \zeta_p(x) + \lambda_0 \Omega_p \hat{\xi}_p^b(x) \\ &= c_f (\hat{\xi}_p^s(x) + \Delta_p^{-1} \hat{\xi}_p^b(x)). \end{aligned} \quad (35)$$

Therefore, the outer-region matching data is given by $\Delta_p^{-1} = \lambda_0 \Omega_p / c_f$. Now we substitute $\xi_f(x)$ and $\hat{\xi}_p^b(x)$ into Eq.(19) to obtain

$$\begin{aligned} &(\hat{\xi}_p^b, \mathcal{L}\xi_f) - (\xi_f, \mathcal{L}\hat{\xi}_p^b)^* \\ &= \lim_{x \rightarrow x_0} f(x) \left[\hat{\xi}_p^{b*} \frac{d\xi_f}{dx} - \xi_f \frac{d\hat{\xi}_p^{b*}}{dx} \right] \\ &= -2f_0 \mu c_f. \end{aligned} \quad (36)$$

By using the relation $\mathcal{L}\xi_f = -\Omega_p \mathcal{L}\hat{\xi}_p^b$, we obtain

$$\frac{1}{c_f} = \frac{2f_0 \mu}{(\xi_f, \mathcal{L}\hat{\xi}_p^b) + \lambda_0 \Omega_p (\hat{\xi}_p^b, \mathcal{L}\hat{\xi}_p^b)}. \quad (37)$$

Substituting Eqs.(32), (33) and (34) into Eq.(37), we get the formula for Δ_p^{-1} expressed by

$$\Delta_p^{-1} = \lambda_0 \frac{2f_0 \mu \Omega_p^2}{\|\xi_{p,0}\|^2 + \lambda_0 [W(\zeta_p, \zeta_p) + \Omega_p^2 (\hat{\xi}_p^b, \mathcal{L}\hat{\xi}_p^b)]}. \quad (38)$$

We see that the matching data Δ_p^{-1} tends to zero as $O(\lambda_0)$ when the plasma approaches the marginal stability.

A singular equation such as Eq.(30) can be numerically solved by using a finite element method. The quadratic form corresponding to Eq.(30) is

$$W(\zeta_p, \zeta_p) + 2(\zeta_p, h) + 2\nu(\zeta_p, \rho \xi_{p,0}), \quad (39)$$

$$h(x) = \rho(x) \xi_{p,0}(x) - \Omega_p \mathcal{L}\hat{\xi}_p^b(x), \quad (40)$$

where the scalar ν is the Lagrange multiplier. By requiring that this quadratic form be stationary for the variations of $\zeta_p(x)$ and ν , we obtain the following equations for $\zeta_p(x)$ and ν :

$$\mathcal{L}\zeta_p(x) - \nu \rho(x) \xi_{p,0}(x) = h(x), \quad (41)$$

$$(\rho \xi_{p,0}, \zeta_p) = 0. \quad (42)$$

Equations (41) and (42) are equivalent to Eq.(30)

because they have the solution of $\nu = 0$. Moreover, they are well posed even if the operator \mathcal{L} is singular. We can apply a finite element method to Eqs.(39) and (40) instead of solving Eq.(30) directly.

As known from the derivation, the present eigenvalue method can also be applied to cases when the plasma is far from the marginal stability. It is not necessary for λ_0 to be "small". However, the present method is not applicable if $\Delta_p = 0$, i.e., the big solution satisfies the boundary condition itself. On the other hand, the boundary value method by Pletzer-Dewar can be applied for the $\Delta_p = 0$ case. So, the two method can be regarded as complementary. We can obtain the matching data in the whole region, $0 \leq |\Delta_p| \leq \infty$, by using the both method.

4. Effects of Truncation of the Big Solution

In this section, we proof that the matching data given by Eq.(38) is unique and invariant against the truncation of the Frobenius series of the big solution.

First, we derive the condition for the existence of the integral $(\hat{\xi}_p^b, \mathcal{L}\hat{\xi}_p^b)$ in Eq.(38). If the Frobenius series for the big solution, Eq.(5), are truncated at the first m terms, we obtain

$$\mathcal{L}\hat{\xi}_p^b = r_m |x - x_0|_p^{-1/2-\mu} (x - x_0)^m + \dots, \quad x \rightarrow x_0,$$

where r_m is a constant. It is easy to see that, for $(\hat{\xi}_p^b, \mathcal{L}\hat{\xi}_p^b)$ to be finite, the truncated big solution has to be chosen at least as

$$\xi_p^b(x) = |x - x_0|_p^{-1/2-\mu}, \quad \text{for } 0 < \mu < \frac{1}{2}, \quad (43)$$

or

$$\begin{aligned} \xi_p^b(x) &= |x - x_0|_p^{-1/2-\mu} (1 + \xi_1(x - x_0)), \\ \text{for } \frac{1}{2} < \mu < 1. \end{aligned} \quad (44)$$

Here we do not consider the degenerate case of $\mu = 1/2$, for simplicity.

Let $\hat{\xi}_{p,\text{new}}^b(x)$ be a truncated big solution expressed by more terms than Eq.(43) for $0 < \mu < 1/2$ or Eq.(44) for $1/2 < \mu < 1$. If we write

$$\hat{\xi}_p^b(x) = \hat{\xi}_{p,\text{new}}^b(x) + \delta\xi(x), \quad (45)$$

$$\delta\xi(x=0) = \delta\xi(x=a) = 0, \quad (46)$$

then we find $\delta\xi(x)$ to be a square integrable and $\delta\xi = o(\hat{\xi}_p^b)$, i.e.,

$$\frac{\delta \xi(x)}{\xi_p^s(x)} \rightarrow 0, \quad x \rightarrow x_0.$$

We decompose $\delta \xi(x)$ into

$$\delta \xi(x) = \epsilon \xi_{p,0}(x) + \eta(x), \quad (\xi_{p,0}, \rho \eta) = 0, \quad (47)$$

$$\eta(x=0) = \eta(x=a) = 0, \quad (48)$$

and compute the changes of Ω_p , $\zeta_p(x)$ and the finite energy part $\zeta_f(x)$. By substituting Eq.(45) into Eq.(30), we get

$$\begin{aligned} \mathcal{L}\zeta_p(x) &= \rho(x)\xi_{p,0}(x) - \Omega_p [\mathcal{L}\hat{\xi}_{p,new}^b(x) \\ &\quad - \epsilon \lambda_0 \rho(x)\xi_{p,0}(x) + \mathcal{L}\eta(x)]. \end{aligned} \quad (49)$$

Then the solubility condition for Eq.(49) is

$$\|\xi_{p,0}\|^2 - \Omega_p(\xi_{p,0}, \mathcal{L}\hat{\xi}_{p,new}^b)(1 - \epsilon \omega) = 0, \quad (50)$$

where

$$\omega = \frac{\lambda_0 \|\xi_{p,0}\|^2}{(\xi_{p,0}, \mathcal{L}\hat{\xi}_{p,new}^b)}. \quad (51)$$

In Eq.(50), we use $(\xi_{p,0}, \mathcal{L}\eta) = 0$. Here we assume $\lambda_0 \neq 0$ because we have nothing to do if $\lambda_0 = 0$. While $\zeta_{p,new}(x)$ has to satisfy the singular equation similar to Eq.(30), which is given by

$$\mathcal{L}\zeta_{p,new}(x) = \rho(x)\xi_{p,0}(x) - \Omega_{p,new} \mathcal{L}\hat{\xi}_{p,new}^b(x), \quad (52)$$

and from the solubility condition for Eq.(52) we have

$$\|\xi_{p,0}\|^2 - \Omega_{p,new}(\xi_{p,0}, \mathcal{L}\hat{\xi}_{p,new}^b) = 0. \quad (53)$$

By comparing Eq.(53) with Eq.(50), we obtain

$$\Omega_{p,new} = \frac{\omega}{\lambda_0} = \Omega_p(1 - \epsilon \omega). \quad (54)$$

By using Eq.(54), we can rewrite Eq.(52) as

$$\mathcal{L}\zeta_{p,new}(x) = (1 - \epsilon \omega) \mathcal{L}\zeta_p(x) + \frac{\omega}{\lambda_0} \mathcal{L}\eta(x). \quad (55)$$

The operator \mathcal{L} in Eq.(55) can be removed because $\zeta_{p,new}(x)$ and $\eta(x)$ are square integral functions satisfying both the same boundary and the same orthogonal conditions. Then we obtain

$$\zeta_{p,new}(x) = (1 - \epsilon \omega) \zeta_p(x) + \frac{\omega}{\lambda_0} \eta(x). \quad (56)$$

Now, it is easy to compute the change of the finite energy part in Eq.(34). It is

$$\xi_{f,new}(x) = (1 - \epsilon \omega) \xi_f(x) + \omega \delta \xi(x). \quad (57)$$

Equation (57) is substituted into the integral relation, Eq.(36), for $c_{f,new}$. The left hand size of it becomes

$$\begin{aligned} &(\hat{\xi}_{p,new}^b, \mathcal{L}\xi_{f,new}) - (\xi_{f,new}, \mathcal{L}\hat{\xi}_{p,new}^b) \\ &= (1 - \epsilon \omega)[(\hat{\xi}_p^b, \mathcal{L}\xi_f) - (\xi_f, \mathcal{L}\hat{\xi}_p^b)] \\ &\quad + \omega[(\hat{\xi}_p^b, \mathcal{L}\delta \xi) - (\delta \xi, \mathcal{L}\hat{\xi}_p^b)]. \end{aligned} \quad (58)$$

However, $(\hat{\xi}_p^b, \mathcal{L}\delta \xi) = (\delta \xi, \mathcal{L}\hat{\xi}_p^b)$ because $\delta \xi = o(\xi_p^s)$ [4]. Therefore, we obtain

$$c_{f,new} = (1 - \epsilon \omega) c_f, \quad (59)$$

and

$$\Delta_{p,new}^{-1} = \frac{\lambda_0 \Omega_{p,new}}{c_{f,new}} = \frac{\lambda_0 \Omega_p}{c_f} = \Delta_p^{-1}. \quad (60)$$

In summary, we obtain a fundamental theorem on the present method:

- the matching data computed by Eq.(38) is unique as long as the infinite energy part is so defined that the integral $(\hat{\xi}_p^b, \mathcal{L}\hat{\xi}_p^b)$ exists.

A similar theorem also holds for the original boundary value method by Pletzer-Dewar.

5. Application to a Model Equation

The eigenvalue method is applied to a model equation:

$$\begin{aligned} \mathcal{L}\xi \equiv \frac{d}{dx} \left(f(x) \frac{d\xi}{dx} \right) - g(x)\xi &= -\lambda \rho(x)\xi, \\ x \in [0, 1], \end{aligned} \quad (61)$$

where functions $f(x)$, $g(x)$ and $\rho(x)$ are given by

$$f(x) = (x - x_0)^2, \quad (62)$$

$$g(x) = (\alpha^2 - \frac{1}{4}) - \beta^2(x - x_0)^2, \quad (63)$$

and

$$\rho(x) = (x - x_0)^2. \quad (64)$$

The big and small solutions for Eq.(61) are analytically expressed by

$$\xi_p^b(x) = \left(\frac{\beta}{2}\right)^\alpha \Gamma(1-\alpha) |x-x_0|_p^{-1/2} J_{-\alpha}(\beta|x-x_0|_p), \quad (65)$$

$$\xi_p^s(x) = \left(\frac{\beta}{2}\right)^{-\alpha} \Gamma(1+\alpha) |x-x_0|_p^{-1/2} J_\alpha(\beta|x-x_0|_p). \quad (66)$$

Here, $J_{\pm\alpha}$ is the Bessel function defined by

$$J_\alpha(x) \equiv \left(\frac{x}{2}\right)^\alpha \sum_{n=0}^{\infty} \frac{(-1)^n (x/2)^{2n}}{n! \Gamma(\alpha+n+1)}, \quad (67)$$

and $\Gamma(\alpha)$ is the gamma function. The Suydam index μ is equal to α for the present case. In the following, we limit ourselves to $p = L$ to specify the problem.

The matching data Δ_L^{-1} is given by

$$\Delta_L^{-1} = -\frac{\xi_L^s(0)}{\xi_L^b(0)} = -\left(\frac{\beta}{2}\right)^{-2\alpha} \frac{\Gamma(1+\alpha)}{\Gamma(1-\alpha)} \frac{J_\alpha(\beta x_0)}{J_{-\alpha}(\beta x_0)}. \quad (68)$$

Therefore, we obtain

$$\Delta_L^{-1} = 0 \text{ for } \beta = \frac{j_{\alpha,n}}{x_0}, \quad (69)$$

and

$$\Delta_L = 0 \text{ for } \beta = \frac{j_{-\alpha,n}}{x_0}, \quad (70)$$

where $j_{\alpha,n}$ is the n -th zero point of the Bessel function J_α . Equation (61) has eigenvalues

$$\lambda_n = \left(\frac{j_{\alpha,n}}{x_0}\right)^2 - \beta^2, \quad (71)$$

and the normalized eigenfunctions given by

$$\xi_{L,n}(x) = \bar{c} t^{-1/2} J_\alpha(\sqrt{\beta^2 + \lambda_{L,n}} t), \text{ for } x < x_0, \quad (72)$$

and $\xi_{L,n}(x) = 0$ for $x > x_0$. Here, $t = |x-x_0|_L$ and the normalization factor \bar{c} is

$$\bar{c} = \left(\int_0^{x_0} t J_\alpha^2(\sqrt{\beta^2 + \lambda_{L,n}} t) dx\right)^{-1/2}. \quad (73)$$

In applying the eigenvalue method to the present problem and the $m = 1$ mode theory, we utilize the lowest hybrid finite elements $\{e_{j+1/2}(x)\}$ [5] defined by

$$e_{j+1/2}(x) = \begin{cases} 1, & \text{for } x_j < x < x_{j+1}, \\ 0, & \text{otherwise.} \end{cases} \quad (74)$$

A function $\xi(x)$ and its derivative $d\xi/dx$ are approximated by

$$\xi(x) = \sum_{j=1}^N \frac{\xi_j + \xi_{j+1}}{2} e_{j+1/2}(x), \quad (75)$$

and

$$\frac{d\xi}{dx} = \sum_{j=1}^N \frac{\xi_{j+1} - \xi_j}{x_{j+1} - x_j} e_{j+1/2}(x), \quad (76)$$

The nodes $\{x_j\}_{j=1, \dots, N+1}$ defined as

$$0 = x_1 < \dots < x_{J-1} < x_{JL} = x_{JR} = x_0 < x_{J+1} < \dots < x_{N+1} = 1, \quad (77)$$

are generated by $x_j = F(j)$ with the generating function

$$F(j) = \begin{cases} x_0 \left[1 - \left(1 - \frac{j-1}{J-1}\right)^\gamma\right], & 1 \leq j < J, \\ x_0, & j = J, \\ x_0 + (1-x_0) \left(\frac{j-J}{N+1-J}\right)^\gamma, & J < j \leq N+1. \end{cases} \quad (78)$$

The parameter γ characterizes the node accumulation around the regular singular point x_0 . Its value for $\alpha < 1/2$ is chosen in such that finite element solutions reproduce the singular behavior at x_0 of the eigenfunction $\xi_{p,0}(x)$ and of the solution $\xi_p(x)$ in Eqs.(41) and (42). Whereas the uniform distribution of the nodes ($\gamma = 1$) suffices for $\alpha \geq 1/2$ because $\xi_{p,0}(x)$ and $\xi_p(x)$ are finite at x_0 .

Equation (61) is reduced by the finite element approximation to a linear equation of the unknown vector (the symbol t denotes transpose of a vector)

$$\vec{\xi} \equiv (\xi_1, \dots, \xi_{JL}, \xi_{JR}, \dots, \xi_{N+1})^t. \quad (79)$$

The natural boundary condition can be imposed by removing the coupling between ξ_{JL} and ξ_{JR} in the linear equation. The boundary condition for Eqs.(41) and (42) can be imposed by the same procedure. A detailed description of solving methods of linear equations reduced by the present method is found in ref.[14].

Figure 1 shows $\xi_{L,0}(x)$ and $\xi_L(x)$ numerically obtained by the eigenvalue method for $\alpha = 3/8$, $\beta = 7.4$ and $x_0 = 0.4$ with $N = 800$ and $\gamma = 2.7$. The singular behavior of $\xi_{L,0}(x)$ and $\xi_L(x)$ at x_0 is well illustrated in Fig.1, which verifies the natural boundary condition at

the singular point, x_0 . The accuracy of the eigenvalue λ_0 and the matching data Δ_L^{-1} obtained by the eigenvalue method is already satisfactory for $N = 800$; they are

$$\lambda_0 = 0.1058341, \quad \Delta_L^{-1} = 0.7235707 \times 10^{-3},$$

and Eqs.(68) and (71) give

$$\begin{aligned} \lambda_0(\text{analytical}) &= 0.1057985, \\ \Delta_L^{-1}(\text{analytical}) &= 0.7233488 \times 10^{-3}, \end{aligned}$$

where the values of the Bessel function $J_\alpha(x)$ are evaluated according to ref.[15].

The present eigenvalue method provides the quadratic convergence property with respect to the node number. Figure 2 shows the dependence of $\delta\lambda$ and the relative error of Δ_L^{-1} to the analytical value, $\delta\Delta_L^{-1}$, on $1/N^2$ for the parameters in Fig.1, where

$$\delta\lambda = \lambda_0 - \lambda_0(\text{analytical}).$$

These results by Figs.1 and 2 demonstrate that the proposed method is satisfactory.

6. Comparison with the $m = 1$ Mode Theory

The $m = 1$ mode provides a theoretically important example for which the eigenvalue method proposed in the present paper is fully exploited. In this section, the analytical results of the Newcomb equation for the $m = 1$ mode are presented for the self-containment although the results are well known [7, 16]. Next, the eigenvalue method is applied to the $m = 1$ mode problem, and numerical results are compared with the theory in detail to verify the proposed method.

6.1 Newcomb Equation for the $m = 1$ mode

When the length and the magnetic field is measured by the longitudinal length (major plasma radius) R_0 and the magnetic fields at the plasma surface B_0 , the Newcomb equation for the $m = 1$ mode is written as

$$\frac{d}{dx} \left(f(x) \frac{d\xi}{dx} \right) - \epsilon^2 g(x) \xi = 0, \quad (80)$$

$$\begin{aligned} f(x) &= \frac{x^3}{1 + \epsilon^2 x^2} \left(\frac{1}{q} - 1 \right)^2 \\ &= f_0(x - x_0)^2 + f_1(x - x_0)^3 + \dots, \quad (81) \end{aligned}$$

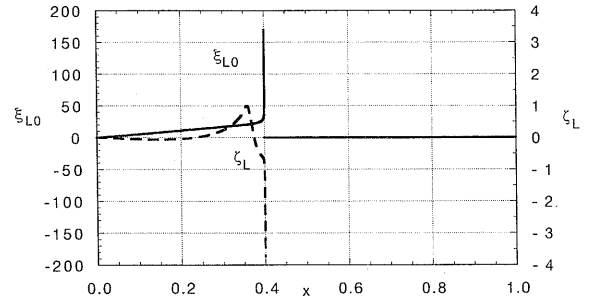


Fig. 1 $\xi_{L0}(x)$ and $\zeta_L(x)$ for $\alpha = 3/8$, $\beta = 7.4$ and $x_0 = 0.4$ with $N = 800$ and $\gamma = 2.7$. The singular behavior of them at x_0 is well illustrated, which verifies the natural boundary condition at x_0 .

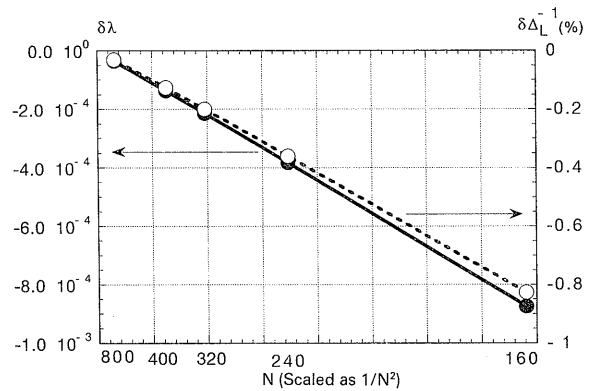


Fig. 2 Dependence of $\delta\lambda$ and $\delta\Delta_L^{-1}$ on $1/N^2$ for the parameters in Fig.1, where $\delta\lambda = \lambda_0 - \lambda_0(\text{analytical})$ and $\delta\Delta_L^{-1}$ is the relative error of Δ_L^{-1} to the analytical value with $\lambda_0(\text{analytical}) = 0.1057985$, and $\Delta_L^{-1}(\text{analytical}) = 0.7233488 \times 10^{-3}$.

$$\begin{aligned} g(x) &= \frac{2x^2}{1 + \epsilon^2 x^2} \left(\frac{1}{\epsilon^2} \frac{dp}{dx} \right) + F^2 \frac{x^3}{1 + \epsilon^2 x^2} \left(\frac{1}{q} - 1 \right) \\ &\times \left[\left(\frac{1}{q} - 1 \right) - \frac{2}{1 + \epsilon^2 x^2} \left(\frac{1}{q} + 1 \right) \right] \\ &= g_0 + g_1(x - x_0) + \dots \quad (82) \end{aligned}$$

Here ξ stands for the radial component of infinitesimal displacement of the plasma, $\epsilon = a/R_0$ with a being the plasma radius, q is the safety factor with $q(x_0) = 1$, F is the longitudinal magnetic field normalized to $F(x = 1) = 1$.

Since $g(x)$ in Eq.(80) is assumed to be $O(1)$, the equilibrium pressure p is

$$\frac{1}{\epsilon^2} \frac{dp}{dx} = O(1) , \quad (83)$$

and

$$\frac{dp}{dx} = O(x) \text{ as } x \rightarrow 0 . \quad (84)$$

The Suydam index μ for Eq.(80) is given by

$$\mu^2 = \frac{1}{4} + \frac{2}{x} \left(\frac{q}{dq/dx} \right)^2 \frac{dp}{dx} \frac{1}{F^2} , \quad (85)$$

and $\mu = 1/2 + O(\epsilon^2)$, that is, the plasma is close to the marginal stability for the $m = 1$ mode due to Eq.(83).

In this work, we employ the fixed boundary condition

$$\xi(x = 1) = 0 , \quad (86)$$

by assuming an ideally conducting wall at the plasma surface. The plasma center ($x = 0$) is the additional regular singular point of the Newcomb equation in a cylindrical plasma and the regularity condition has to be imposed at $x = 0$; for the $m = 1$ mode, it is

$$\frac{d\xi}{dx} = 0 , \text{ at } x = 0 . \quad (87)$$

We first study the solution for $x < x_0$. For $\epsilon = 0$, Eq.(80) has the solution

$$\xi_L(x) = \begin{cases} 1 , & \text{for } x < x_0 , \\ 0 , & \text{for } x > x_0 , \end{cases} \quad (88)$$

which is the small solution for the marginally stable state of $\lambda = 0$. Therefore, the eigenvalue in $O(\epsilon^2)$ is given by

$$\lambda = \epsilon^2 c , \quad (89)$$

$$c = \frac{\int_0^{x_0} g(x) dx}{\int_0^{x_0} \rho(x) dx} . \quad (90)$$

Equation (90) implies that in $O(\epsilon^2)$ the plasma is unstable against the $m = 1$ mode when $q(x)$ is an increasing function with $q_0 = q(x=0) < 1$ (ideal $m = 1$ internal kink instability). Such a profile makes $g(x)$ negative for $x < x_0$ yielding a negative eigenvalue.

Let us compute the $O(\epsilon^2)$ correction to Eq.(88). Substituting $\xi_L(x) = 1 + \epsilon^2 \zeta_L(x)$ into Eq.(80) we obtain

$$\frac{d}{dx} \left(f(x) \frac{d\zeta_L}{dx} \right) = g(x) . \quad (91)$$

By using the regularity condition, Eq.(87), we have

$$\zeta_L(x) = \int_0^x \frac{w(z)}{f(z)} dz , \quad (92)$$

where

$$w(x) = \int_0^x g(z) dz . \quad (93)$$

On deriving Eq.(92) we used the relation $g(x) = O(x^3)$ as $x \rightarrow 0$ obtained from Eqs.(82) and (84).

Let x_1 be a point such that functions $f(x)$ and $w(x)$ can be expanded for $x_1 < x < x_0$ as

$$\frac{1}{f(x)} = \frac{f_2}{(x-x_0)^2} + \frac{f_{-1}}{x-x_0} + f_r(x) , \quad (94)$$

$$w(x) = w_0 + w_1(x-x_0) + \dots , \quad (95)$$

where $f_r(x)$ is analytic at x_0 . By using Eqs.(94) and (95) in Eq.(92) we obtain

$$\begin{aligned} \zeta_L(x) &= \int_0^{x_1} \frac{w(z)}{f(z)} dz + \int_0^{x_1} \frac{w_0 f_{-2}}{(x-x_0)^2} dz \\ &+ \int_0^{x_1} \frac{w_0 f_{-1} + w_1 f_{-2}}{x-x_0} dz + \int_0^{x_1} w_r(z) dz \\ &= \frac{w_0 f_{-2}}{x_0 - x} + (w_0 f_{-1} + w_1 f_{-2}) \log(x_0 - x) \\ &+ \zeta_{Lr}(x) , \end{aligned} \quad (96)$$

where $w_r(x)$ and $\zeta_{Lr}(x)$ are functions analytic at x_0 . Equation (96) gives the expression of $\zeta_L(x)$ valid in the interval $x_1 \leq x < x_0$. The first two terms in the right hand side of Eq.(96) represent the big solution contained in $\zeta_L(x)$. The log function in Eq.(96) implies that the big solution is *redefined* [4] (see also Appendix A). From Eq.(96) and the relation $f_{-2} = 1/f_0$, we have the matching data given by

$$\hat{\Delta}_L^{-1} = \epsilon^2 \frac{w_0}{f_0} = \frac{\epsilon^2}{f_0} \int_0^{x_0} g(x) dx , \quad (97)$$

where the symbol “ $\hat{\Delta}$ ” denotes the matching data for the redefined big solution.

Let us next study Eq.(80) for $x > x_0$. We limit ourselves to the case of $\epsilon = 0$ for simplicity. The corresponding eigenvalue problem cannot be analytically solved and has to invoke the numerical method. The right side solution $\xi_R(x)$ satisfying the boundary condition $\xi_R(1) = 0$ is

$$\xi_R(x) = a \int_1^x \frac{dy}{f(y)} , \quad (98)$$

where a is an arbitrary constant. Since $f(x) > 0$ for $x > x_0$, the expansion of $1/f(x)$ given by Eq.(94) is valid in the interval $x_0 < x \leq 1$. Therefore, the solution $\xi_R(x)$ can be written as

$$\xi_R(x) = a \left[-\frac{f_{-2}}{x-x_0} + f_{-1} \log(x-x_0) + d_0 + h_r(x) \right], \quad (99)$$

where

$$d_0 = \frac{f_{-2}}{1-x_0} - f_{-1} \log(1-x_0) - \int_{x_0}^1 f_r(x) dx, \quad (100)$$

and

$$h_r(x) = \int_{x_0}^x f_r(z) dz, \quad h_r(x_0) = 0. \quad (101)$$

The big solution in Eq.(99) is

$$\xi_R^b(x) = - \left[\frac{1}{x-x_0} + \frac{f_1}{f_0} \log(x-x_0) + \dots \right]. \quad (102)$$

Since the small solution behaves as $\xi_R^s(x) = 1 + \dots$ as $x \rightarrow x_0$, we have the right side matching data given by

$$\hat{\Delta}_R = -\frac{d_0}{f_{-2}} = -\frac{1}{1-x_0} - \frac{f_1}{f_0} \log(1-x_0) + f_0 \int_{x_0}^1 f_r(x) dx. \quad (103)$$

6.2 Numerical Experiments

The safety factor used in the numerical experiments has the functional form of

$$q(x) = q_0 \left[1 + \left(\frac{x}{x_0} \right)^a \right]^b, \quad (104)$$

where q_0 is the safety factor at the axis, x_0 is the position of the $q = 1$ surface. The parameter b is given by

$$b = \frac{\log(1/q_0)}{\log 2},$$

from the prescribed value of q_0 . The parameters used in the present study are $q_0 = 0.9$, $x_0 = 0.5$ and $a = 4$, and Fig.3 shows the profiles of $q(x)$ (solid line) and dq/dx (dotted line).

The pressure gradient dp/dx is determined so that the Suydam index given by Eq.(85) is uniform in the plasma. Then we have

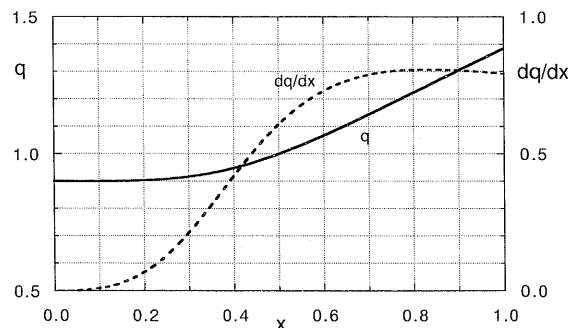


Fig. 3 Profiles of $q(x)$ (solid line) and dq/dx (dotted line) for $q_0 = 0.9$, $x_0 = 0.5$ and $a = 4$.

$$\frac{dp}{dx} = - \left(\frac{1}{4} - \mu^2 \right) \frac{x}{2} F^2 \left(\frac{dq/dx}{q} \right)^2. \quad (105)$$

We also impose the relation

$$\mu = \frac{1}{2} \sqrt{1 - \epsilon^2}, \quad (106)$$

to meet the assumption, Eq.(83). From the equilibrium relation, the longitudinal magnetic field F satisfies the equation

$$\frac{1}{\epsilon^2} \frac{dF^2}{dx} = - \frac{2}{1 + \epsilon^2 (x/q)^2} \left(\frac{1}{\epsilon^2} \frac{dp}{dx} + \frac{F^2}{q} \frac{d}{dx} \left(\frac{x^2}{q} \right) \right), \quad (107)$$

and the boundary condition

$$F^2(x=1) = 1. \quad (108)$$

By solving Eq.(107) with Eq.(105) and Eq.(108) we obtain the longitudinal magnetic field $F(x)$.

On applying the eigenvalue method to the Newcomb equation for the $m = 1$ mode, we use the re-defined big solution because the Suydam index is close to $1/2$. We also change the unknown variable $\xi(x)$ to $Y(x) = x\xi(x)$ since the regularity condition for $Y(x)$ at the plasma center ($x = 0$),

$$Y(x) = 0, \quad (109)$$

is convenient for the finite element method. The matching data is invariant on such change of the variable as long as the big solution is not redefined. When the re-defined big solution is used, the transformation law between the matching data $\hat{\Delta}_p$ for $Y(x)$ and $\hat{\Delta}_p$ for $\xi(x)$ reads

$$\bar{\Delta}_R = \hat{\Delta}_R + \frac{1}{x_0}, \quad \bar{\Delta}_L = \hat{\Delta}_L - \frac{1}{x_0}. \quad (110)$$

The derivation of Eq.(110) is given in Appendix B.

Finally, the weight function for the eigenvalue problem corresponding to Eq.(80) is chosen as

$$\rho(x) = F^2 x^2 \left(\frac{1}{q} - 1 \right)^2. \quad (111)$$

Figure 4 shows the ϵ^2 dependence of the first left side eigenvalue λ_L . The symbols “×” and “○” are for eigenvalues numerically obtained with $N = 200$ and calculated by Eqs.(89) and (90), respectively. The agreement between the two is excellent:

$$\begin{aligned} \lambda_L(\text{numerical}) &= -0.05388804, \\ \lambda_L(\text{analytical}) &= -0.05401794, \end{aligned}$$

for $\epsilon = 0.05$. The left side eigenvalue is negative and it implies that the ideal $m = 1$ mode is unstable. Figure 5 shows the ϵ^2 dependence of the first right side eigenvalue λ_R ($N = 200$). The right side eigenvalue is positive, which, of course, means the $m = 1$ mode is stable in the region of $x > x_0$. We illustrate in Fig.6 the first eigenfunctions, $Y_{L0}(x)$ and $Y_{R0}(x)$, in the left and the right sides for $\epsilon = 0.05$ and $N = 200$. The profile of $Y_{L0}(x)$ is nearly straight according to Eq.(88).

Figure 7 shows the left side matching data $\bar{\Delta}_L^{-1}$ obtained by the eigenvalue method (symbol “○”) with $N = 200$ and by Eq.(97) (symbol “×”). The matching data computed by Eq.(97) for $\xi(x)$ is transformed to the matching data for $Y(x)$ according to Eq.(110). The matching data for $\epsilon = 0.05$ is

$$\begin{aligned} \bar{\Delta}_L^{-1}(\text{numerical}) &= -0.2097123 \times 10^{-3}, \\ \bar{\Delta}_L^{-1}(\text{analytical}) &= -0.2112248 \times 10^{-3}. \end{aligned}$$

The right side matching data $\bar{\Delta}_R$ is shown in Fig.8 ($N = 200$). The matching data computed by Eq.(103) depicted by the symbol “●” is

$$\bar{\Delta}_R = 15.32481,$$

while the eigenvalue method gives

$$\bar{\Delta}_R = 15.30819,$$

for $\epsilon = 0.05$. Figure 9 shows $\zeta_p(x)$ ($p = L, R$), the finite element solutions of Eq.(30) for $\epsilon = 0.05$ and $N = 200$, where the redefined big solution is used.

Next, let us see the convergence property of the present method. Figures 10 and 11 show the dependence of eigenvalues in the left and right sides for $\epsilon = 0.05$, respectively, on the grid number N . Figure 12 shows the convergence of $\bar{\Delta}_L^{-1}$ with respect to $1/N^2$

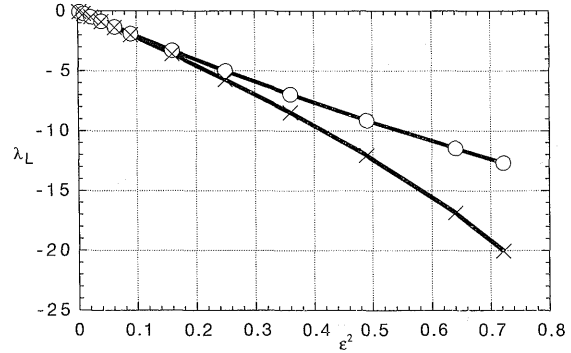


Fig.4 ϵ^2 dependence of the first left side eigenvalue λ_L . The symbol “×” is numerically obtained eigenvalue with $N = 200$ and “○” is for the eigenvalue calculated by Eqs.(89) and (90).

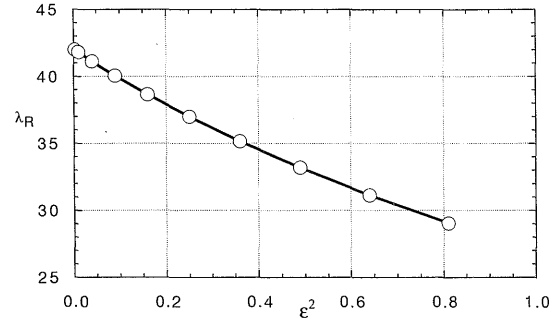


Fig.5 ϵ^2 dependence of the first right side eigenvalue λ_R with $N = 200$.

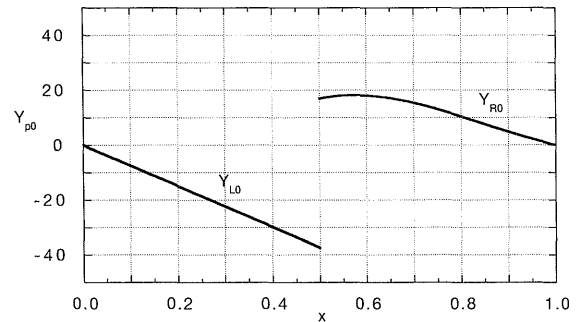


Fig.6 The first eigenfunctions, $Y_{L0}(x)$, in the left side, which is nearly straight according to Eq.(88), and $Y_{R0}(x)$ in the right side for $\epsilon = 0.05$ and $N = 200$.

($\epsilon = 0.05$), where $\bar{\Delta}_L^{-1}$ is normalized to ϵ^2 . These results confirm the quadratic convergence property of the present method for the Newcomb equation.

Finally, we compare our eigenvalue method with the boundary value method by Pletzer-Dewar [4].

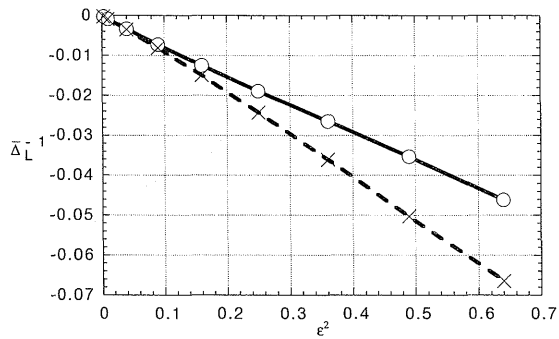


Fig. 7 Left side matching data $\bar{\Delta}_L^{-1}$ obtained by the eigenvalue method (symbol "○") and by Eq.(97) (symbol "×"). The redefined big solution is used on applying the eigenvalue method. Also, the matching data computed by Eq.(97) is transformed to the matching data for $Y(x)$ according to Eq.(110).

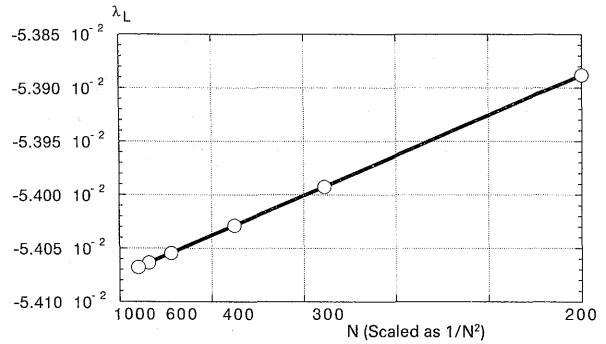


Fig. 10 Dependence of the left eigenvalue λ_L for $\epsilon = 0.05$ on the grid number N .

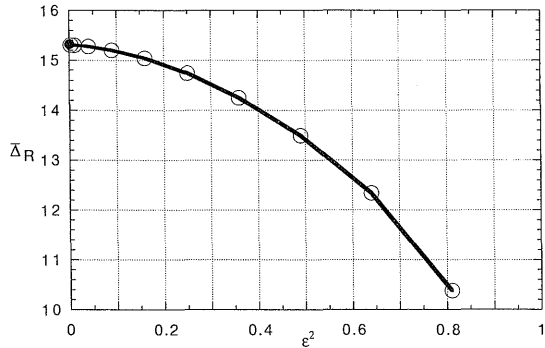


Fig. 8 Right side matching data $\bar{\Delta}_R(N = 200)$. The symbol "●" depicts the matching data computed by Eq.(103).

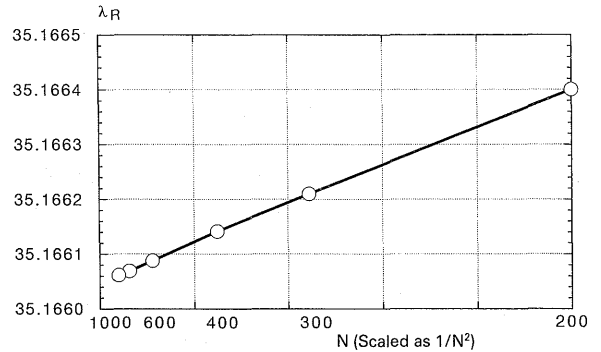


Fig. 11 Dependence of the right eigenvalue λ_R for $\epsilon = 0.05$ on the grid number N .

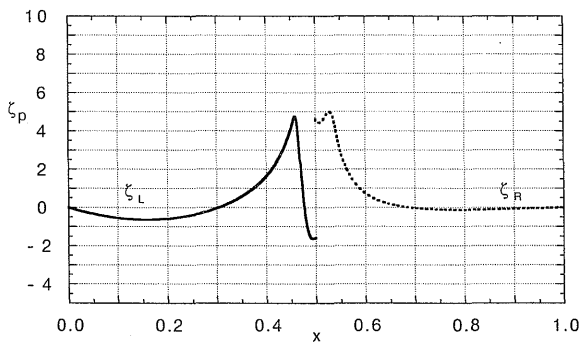


Fig. 9 Finite element solutions of Eq.(30), $\zeta_p(x)$ ($p = L, R$), for $\epsilon = 0.05$, $N = 200$.

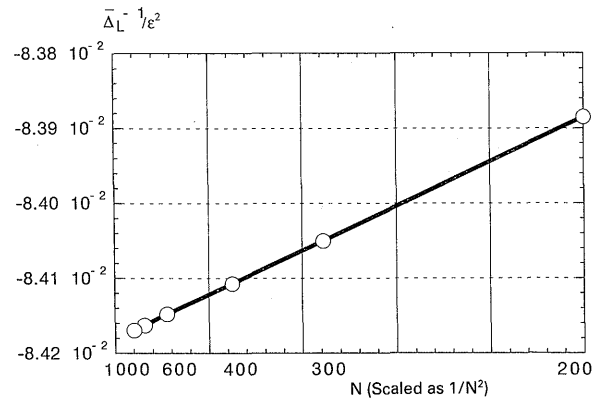


Fig. 12 Convergence of $\bar{\Delta}_L^{-1}$ with respect to $1/N^2$ for $\epsilon = 0.05$.

Figure 13 shows the dependence of the right matching data $\bar{\Delta}_R$ on N for $\epsilon = 0.6$ ($\mu = 0.4$). The symbol "●" is for the eigenvalue method, and "○" for the boundary

value method when the Frobenius series truncated at the first term is used for the big solution. While the black and white "△"s are for, respectively, the eigen-

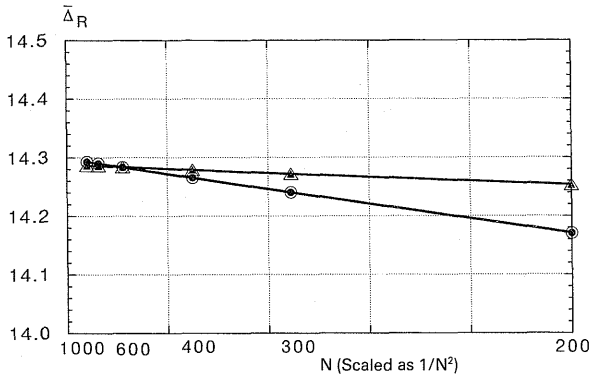


Fig. 13 Dependence of the right matching data Δ_R on N for $\epsilon = 0.6$ ($\mu = 0.4$). The symbol "●" is for the eigenvalue method, and "○" for the boundary value method when the Frobenius series truncated at the first term is used for the big solution. The black and white "△"s are for, respectively, the eigenvalue and boundary value methods when the redefined big solution is used.

value and boundary value methods when the redefined big solution is used. The matching data by the eigenvalue method well coincide with those by the boundary value method for the both cases. All cases converge to the same value quadratically with respect to $1/N^2$. These results demonstrate the theorem on the truncation of the big solution given in Sec. 4.

7. Conclusions and Discussion

The contribution of the eigenvalue method proposed in the present work to the MHD stability theory is twofold. First, the method provides a new method of the ideal MHD stability analysis, which can identify the marginally stable state against ideal MHD motion. Second, by using the present method, the outer-region matching data can be computed for a plasma close to the ideal MHD stability limit. Both imposing the natural boundary condition at the rational surface and defining the appropriate weight function play a crucial role in the formulation of the eigenvalue method. Due to such a formulation, the spectra of the equation to be solved comprise of the point spectra (eigenvalues) without the continuous spectra.

Acknowledgments

The authors wish to thank Profs. T. Ushijima and T. Kako at the university of electro-communications for their valuable comments on the present work. The authors are also grateful to Dr. Masafumi Azumi and Dr. Toshio Hirayama at JAERI for their encouragement.

Appendix A: Redefinition of the Big Solution

When the Suydam index μ is equal or close to $1/2$, it is necessary to redefine the big solution. The Frobenius series of the big solution up to the second term is

$$\xi_p^b(x) = t_p^{-1/2-\mu} + s(\mu) \text{sgn}(t) t_p^{1/2-\mu};$$

$$t = x - x_0, \tag{112}$$

where

$$s(\mu) = -\frac{s_{-1}}{2} \frac{1}{\delta\mu} - \frac{f_1}{2f_0} \delta\mu, \tag{113}$$

$$s_{-1} = \frac{f_1 + g_1}{f_0}, \tag{114}$$

and $\delta\mu = \mu - 1/2$; f_0, f_1 and g_1 are given in Eqs.(81) and (82). Then the redefined big solution is given by

$$\xi_p^b(x) \equiv t_p^{-1/2-\mu} + s(\mu) \text{sgn}(t) (t_p^{1/2-\mu} - t_p^{-1/2+\mu}). \tag{115}$$

The second term in the right hand of Eq.(115) for $\mu \rightarrow 1/2$ becomes

$$\lim_{\mu \rightarrow 1/2} s(\mu) (t_p^{1/2-\mu} - t_p^{-1/2+\mu}) = s_{-1} \log t_p, \tag{116}$$

and the linear independence between the big and small solutions is retained. From Eq.(112) we obtain the relation between the matching data $\hat{\Delta}_p$ when the redefined big solution is used and the data Δ_p for the original big solution:

$$\hat{\Delta}_R = \Delta_R + s(\mu), \quad \hat{\Delta}_L = \Delta_L - s(\mu), \tag{117}$$

and we see that the original matching data becomes infinity as $\mu \rightarrow 1/2$, while the redefined matching data remains finite.

Appendix B: Transformation of the Matching Data

The Suydam index is unchanged on the transformation of the unknown variable from $\xi(x)$ to $Y(x) \equiv x\xi(x)$. It is also easy to see that the matching data are invariant on such transformation if $2\mu \neq \text{integer}$. Let us consider the case of $\mu = 1/2$. The Frobenius series of the big and small solutions for $x > x_0$ have the forms of

$$\xi_R^b(x) = \frac{1}{x - x_0} + \alpha \log(x - x_0) [1 + P(x - x_0)] + Q(x - x_0), \tag{118}$$

$$\xi_R^s(x) = 1 + R(x - x_0), \quad (119)$$

where α is a constant, and each of $P(t)$, $Q(t)$ and $R(t)$ is a function expressed by the power series of t without including a constant [17]. Therefore, we have

$$x \xi_R^b(x) = x_0 \left\{ \frac{1}{x_0} + \frac{1}{x - x_0} + \alpha \log(x - x_0) [1 + \tilde{P}(x - x_0)] + \tilde{Q}(x - x_0) \right\}, \quad (120)$$

and

$$x \xi_R^s(x) = x_0 [1 + \tilde{R}(x - x_0)]. \quad (121)$$

Here, $\tilde{P}(t)$, $\tilde{Q}(t)$ and $\tilde{R}(t)$ are again functions expressed by the power series of t without constants. We see in Eq.(120) that $x \xi_R^b(x)$ is a mixture of the big solution, $\Xi_R^b(x)$, and the small solution, $\Xi_R^s(x)$, for $Y(x)$:

$$x \xi_R^b(x) \propto \Xi_R^b(x) + \frac{1}{x_0} \Xi_R^s(x). \quad (122)$$

Therefore, we obtain the transformation law between the matching data $\hat{\Delta}_R$ for $\xi(x)$ and the matching data $\bar{\Delta}_R$ for $Y(x)$,

$$\bar{\Delta}_R = \hat{\Delta}_R + \frac{1}{x_0}. \quad (123)$$

Similarly, we have

$$\bar{\Delta}_L = \hat{\Delta}_L - \frac{1}{x_0}. \quad (124)$$

Next, let us consider the case of the big solution redefined according to Eq.(115). Let $s(\mu)$ and $\hat{s}(\mu)$ be the right hand side in Eq.(113) for $Y(x)$ and $\xi(x)$. Then, by the same reason in Eq.(118), we have

$$\hat{s}(\mu) = s(\mu) - \frac{1}{x_0}. \quad (125)$$

By using Eq.(125) in Eq.(117) and the invariance property of the matching data Δ_p for $2\mu \neq$ integer, we have

$$\bar{\Delta}_R = \hat{\Delta}_R + \frac{1}{x_0}, \quad \bar{\Delta}_L = \hat{\Delta}_L - \frac{1}{x_0}. \quad (126)$$

Thus, the transformation law for the redefined big solution remains unchanged even for $\mu \rightarrow 1/2$. Notice that the matching data computed by the MARG1D code are $\bar{\Delta}_p$ and the data given by the $m = 1$ mode theory are $\hat{\Delta}_p$.

References

- [1] H.P. Furth, J. Killeen and M.N. Rosenbluth, Phys. Fluids **6**, 459 (1963).
- [2] B. Coppi, J.M. Greene and J.L. Johnson, Nuclear Fusion **6**, 101 (1966).
- [3] W.A. Newcomb, Annals of Phys. **10**, 232 (1960).
- [4] A. Pletzer and R.L. Dewar, J. Plasma Phys. **45**, 427 (1991).
- [5] R. Gruber and J. Rappaz, *Finite Element Methods in Linear Ideal Magnetohydrodynamics* (Springer-Verlag, Berlin, 1985).
- [6] A. Pletzer, A. Bondeson and R.L. Dewar, J. Comput. Phys. **45**, 427 (1991).
- [7] G. Ara, B. Basu, B. Coppi, G. Laval, M.N. Rosenbluth and B.V. Waddell, Annals of Phys. **112**, 443 (1978).
- [8] R.D. Hazeltine and J.D. Meiss, *Plasma Confinement* (Addison-Wesley, New York, 1992).
- [9] R.L. Dewar and M. Persson, Phys. Fluids B **5**, 4273 (1993).
- [10] R. Courant and D. Hilbert, *Methods of Mathematical Physics* (Interscience, New York, 1953) Vol.1.
- [11] K. Appert, D. Berger, R. Gruber, F. Troyon and K.V. Roberts, Comput. Phys. Commun. **10**, 11 (1975).
- [12] R. Gruber, F. Troyon, D. Berger, L.C. Bernard, S. Rousset, R. Schreiber, W. Kerner, W. Schneider and K.V. Roberts, Comput. Phys. Commun. **21**, 323 (1975).
- [13] R.C. Grim, J.M. Greene and J.L. Johnson, *Computation of the Magnetohydrodynamic Spectrum in Axisymmetric Toroidal Configuration Systems in Methods in Computational Physics* (Springer-Verlag, Berlin, 1985).
- [14] S. Tokuda and T. Watanabe, *MARG1D: One Dimensional Outer Region Matching Data Code*, JAERI-Data/Code 95-011 (1995) [in Japanese].
- [15] W.H. Press, S.A. Teukolsky, W.T. Vetterling and B.P. Flannery, *Numerical Recipes in Fortran* (Cambridge, New York, 1992) 2nd ed., Chap. 6.
- [16] M.N. Rosenbluth, R.Y. Dagazian and P.H. Rutherford, Phys. Fluids **16**, 1894 (1973).
- [17] C.M. Bender and S.A. Orszag, *Advanced Mathematical Methods for Scientists and Engineers* (McGraw-Hill, New York, 1978), Chap. 3.